



HAL
open science

Doping induced stable room temperature dual emission from gadolinium doped vacancy ordered double halide perovskite, Gd:Cs₂SnCl₆

Aadil Ahmad Bhat, Nitesh Singh, Rajesh V Nair, Erik Dujardin, Jadab Sharma

► **To cite this version:**

Aadil Ahmad Bhat, Nitesh Singh, Rajesh V Nair, Erik Dujardin, Jadab Sharma. Doping induced stable room temperature dual emission from gadolinium doped vacancy ordered double halide perovskite, Gd:Cs₂SnCl₆. *Optical Materials*, 2023, 141, pp.113937. 10.1016/j.optmat.2023.113937. hal-03781995

HAL Id: hal-03781995

<https://hal.science/hal-03781995v1>

Submitted on 20 Sep 2022

HAL is a multi-disciplinary open access archive for the deposit and dissemination of scientific research documents, whether they are published or not. The documents may come from teaching and research institutions in France or abroad, or from public or private research centers.

L'archive ouverte pluridisciplinaire **HAL**, est destinée au dépôt et à la diffusion de documents scientifiques de niveau recherche, publiés ou non, émanant des établissements d'enseignement et de recherche français ou étrangers, des laboratoires publics ou privés.

1
2
3
4 **Doping induced stable room temperature dual emission from gadolinium**
5 **doped vacancy ordered double halide perovskite, Gd:Cs₂SnCl₆**
6
7
8

9
10 Aadil Ahmad Bhat¹, Nitesh Singh², Rajesh V. Nair², Erik Dujardin³ and Jadab Sharma^{1*}
11

12
13 Aadil Ahmad Bhat (ID 0000-0002-7510-9663), Dr. Jadab Sharma (ID 0000-0003-3138-8530)
14

15 ¹Centre for Nanoscience and Nanotechnology, Panjab University, Chandigarh-160014, Chandigarh,
16
17 India
18

19 *E-mail: jadabs@pu.ac.in
20
21

22
23 Nitesh Singh (ID 0000-0003-2416-7406), Dr. Rajesh V. Nair (ID 0000-0001-5564-7264)
24

25 ²Department of Physics, Indian Institute of Technology Ropar, Rupnagar-140001, Punjab, India
26
27 Dr. Erik Dujardin (ID 0000-0001-7242-9250)
28

29 ³Laboratoire Interdisciplinaire Carnot de Bourgogne (ICB), CNRS UMR 6303, Université
30
31 Bourgogne Franche-Comté
32

33 9 avenue A. Savary - BP 47870 - 21078 Dijon Cedex - FRANCE
34
35
36

37 **Conflict of interest disclosure**
38

39 The authors declare no conflict of interest.
40
41
42
43

44 **Abstract**
45

46 The recent advancement in bandgap engineering through controlled doping has widened the prospect
47
48 of vacancy ordered double halide perovskites (VO DHPs) by conferring them with designable
49
50 optoelectronic properties. Here, we report synthesis of Gd doped Cs₂SnCl₆ via a simple
51
52 solvothermal method. Gd³⁺ ions doping lowers the band gap from 3.8 eV to 2.8 eV and facilitates
53
54 stable room temperature dual PL emission centered at 440 nm and 610 nm. The macroscopic
55
56 emission process is well supported by the confocal PL emission studies on isolated crystallites.
57
58
59
60
61
62
63
64
65

1
2
3
4 Both the pristine (Cs_2SnCl_6) and $\text{Gd}:\text{Cs}_2\text{SnCl}_6$ exhibit crystalline cubic structure with $Fm\bar{3}m$ space
5
6 group. Rietveld refinement correlates well with the cubic phase and the analysis of (220) XRD
7
8 peak validates the existence of a secondary crystalline phase. SEM studies confirm the anisotropic
9
10 growth, forming large micron sized octahedral structures of pristine ($> 20 \mu\text{m}$) and $\text{Gd}:\text{Cs}_2\text{SnCl}_6$
11
12 ($< 5 \mu\text{m}$). This study enhances the experimental understanding of hitherto unknown dual PL
13
14 emission properties of $\text{Gd}:\text{Cs}_2\text{SnCl}_6$ having implication in quantum photonics leaving a scope for
15
16 detail theoretical study on the origin of the electronic transitions.
17
18
19
20
21
22
23
24

25 **Keywords**

26
27
28 vacancy ordered (VO) double halide perovskites (DHP), band gap engineering,
29
30 photoluminescence (PL) emission, confocal PL spectroscopy.
31
32
33
34
35
36
37
38
39
40
41
42
43
44
45
46
47
48
49
50
51
52
53
54
55
56
57
58
59
60
61
62
63
64
65

1. Introduction

Nano-and micro-crystalline lead halide perovskites (LHP) are considered to be the most prominent and promising photonic materials for optoelectronic and photovoltaic applications.¹⁻⁵ Among them, methyl ammonium lead halide perovskites ($\text{CH}_3\text{NH}_3\text{PbX}_3$)^{5,6} and cesium lead halide perovskites (CsPbX_3),^{7,8} where $X = \text{Cl}, \text{Br}, \text{I}$ have been extensively studied recently due to their exceptional physical and chemical properties. However, in spite of their exciting properties, the commercial prospects of these materials is seriously hampered by the environmental concern of Pb toxicity and their inherent instability. To overcome it, Pb is being replaced with elements such as Sb, Sn, In, Bi, etc.^{9,10} For instance, two Pb^{2+} ions can be replaced by one monovalent metal ion (M^+ : $\text{Li}^+, \text{Ag}^+, \text{Na}^+, \text{K}^+$, etc.) and one trivalent metal ion (M^{3+} : $\text{In}^{3+}, \text{Sb}^{3+}, \text{Bi}^{3+}$) by co-substitution method with the structure $\text{Cs}_2\text{M}^+\text{M}^{3+}\text{X}_6$ ($X = \text{Cl}, \text{Br}, \text{I}$).¹¹⁻¹³ Another feasible strategy is replacement of Pb^{2+} with Sn^{2+} ions, but it also undergoes oxidation to Sn^{4+} .¹⁴ Interestingly, a new class of materials with the stable structure Cs_2SnX_6 , known as vacancy ordered double halide perovskites (VO DHP), has emerged by direct replacement of Pb^{2+} with Sn^{4+} ions.¹⁵

The peculiar crystal structure of Cs_2SnX_6 presents vacancies in B-sites of regular ABX_3 perovskites to form corner sharing $[\text{BX}_6]$ octahedra that shows good thermal and structural stability.¹⁶⁻¹⁹ In this homologous family, Cs_2SnI_6 shows ambipolar characteristics due to p-type and n-type doping depending on cesium or iodide vacancies with an impressive direct band gap of ~ 1.3 eV and good defect tolerance towards vacancy states.^{16,20-22} In contrast, Cs_2SnCl_6 does not show similar optoelectronic properties, thanks to the large band gap (> 3.8 eV), despite exhibiting good thermal and structural stability.¹⁷⁻¹⁹

Recently, bandgap engineering upon doping has widen the prospect of these materials by conferring them with designable optoelectronic properties.²³ For example, blue²⁴, yellow and white²⁵ emission from Cs_2SnCl_6 nanocrystals doped with Bi^{3+} , Te^{4+} , and Sb^{3+} ions, respectively

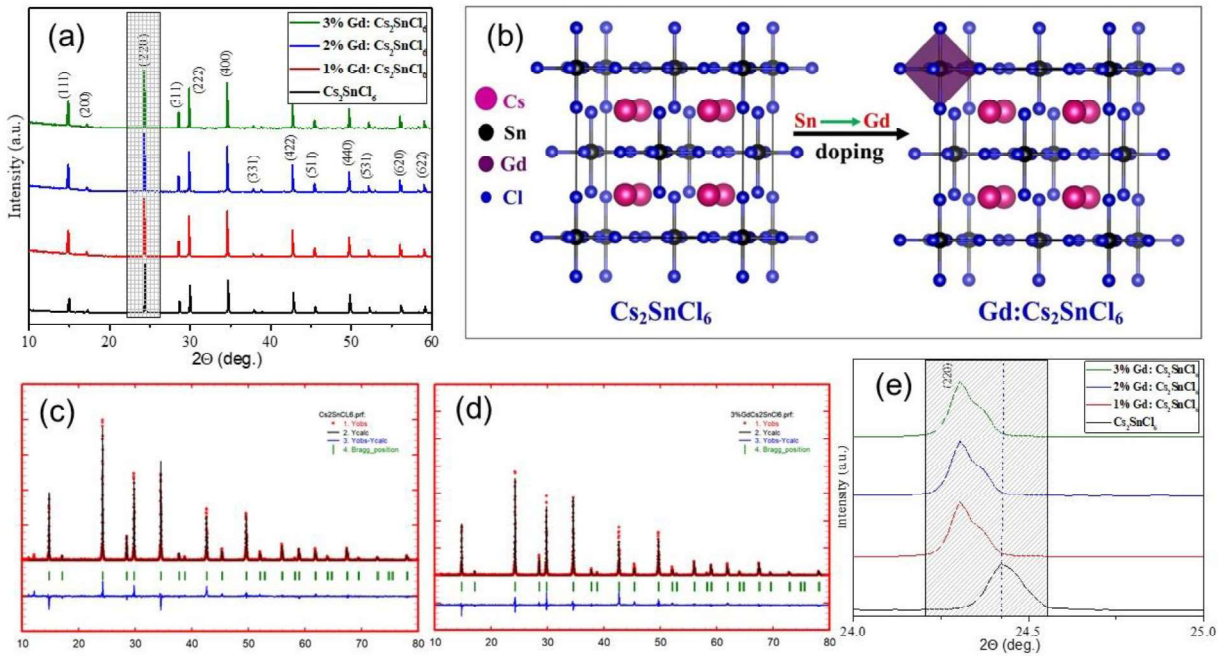
1
2
3
4 have been reported with high quantum yield. Similarly, careful control of the concentration of Sn^{2+}
5
6 in Bi^{3+} -doped Cs_2SnCl_6 leads to blue emission,²⁴ while Sb^{3+} doping produces orange emission.²⁶
7
8 At cryogenic temperature, Sb^{3+} doped Cs_2SnCl_6 shows two emission peaks, while Bi^{3+} doping
9
10 shows only a single peak.²⁷ Very recently, significant alteration of the structural characteristics of
11
12 VO DHPs has been shown by applied pressure opening another leverage to modulate
13
14 optoelectronic properties.²⁸ Thus, renewed research interest on VO DHPs has emerged mainly due
15
16 to their untapped photophysical properties as a result of controlled alteration of crystal structure
17
18 and/or electronic structure by band gap engineering through doping.
19
20
21
22
23

24
25 Herein, we report the anisotropic growth of microcrystalline Gd-doped Cs_2SnCl_6 that shows stable
26
27 dual PL emission even at room temperature. The macroscopic PL emission is corroborated by the
28
29 confocal PL emission studies for isolated crystallites. Our study opens up the possibility of
30
31 lanthanide doping in Cs_2SnCl_6 that requires in-depth theoretical understanding due to the lesser
32
33 explored complex electronic transitions involving electrons in f-orbitals.
34
35
36
37

38 **2. Results and Discussion**

39
40 The crystal structures of Cs_2SnCl_6 and Gd-doped Cs_2SnCl_6 ($\text{Gd}:\text{Cs}_2\text{SnCl}_6$) were assessed by
41
42 powder X-ray diffraction studies as shown in Figure 1a. The emergence of the crystalline cubic
43
44 phase is well correlated with the JCPDS (card No. # 9023) which shows the space symmetry of
45
46 $Fm\bar{3}m$ and the diffraction patterns can be indexed to (111), (200), (220), (311), (222), (400), etc.
47
48 planes of Cs_2SnCl_6 crystalline phase.²⁴ Figure 1b shows the representative crystal structures of
49
50 Cs_2SnCl_6 and $\text{Gd}:\text{Cs}_2\text{SnCl}_6$. It is evident from the XRD patterns that the as-synthesized materials
51
52 have no crystalline impurity diffractions. The Rietveld refinement for Cs_2SnCl_6 and 3 %
53
54 $\text{Gd}:\text{Cs}_2\text{SnCl}_6$ are shown in **Figure 1c & d**, respectively with a very low χ^2 value (< 4.5) indicating
55
56 a good agreement between simulated and experimental XRD patterns (Rietveld refinements for
57
58
59
60
61
62
63
64
65

1
2
3
4 1% Gd:Cs₂SnCl₆ and 2 % Gd:Cs₂SnCl₆ are given as supporting information, SI Figure-S1). The
5
6 XRD patterns for Gd:Cs₂SnCl₆ are identical to that of pristine sample and the peak positions also
7
8 coincide (both experimental and simulated) showing no additional diffraction peaks except the
9
10 splitting of the peak corresponding to (220) plane and a minor shift towards lower 2 Θ value (Figure
11
12 1e). The deviation in the (220) diffraction peak is due to the marginal difference in the ionic radii
13
14 of Gd³⁺ (0.62 Å) and Sn⁴⁺ (0.69 Å) ions in the lattice and creation of halide vacancies arising from
15
16 the charge disparity.^{20,24,29} It is apparent that, as the molar percentage (number of Gd³⁺ ions in the
17
18 crystal) is increased, the crystal structure is deformed and a secondary phase appears. The obtained
19
20 lattice parameters (SI, Table-S1) are in good agreement with the previous reports.²⁴ No noticeable
21
22 degradation could be detected in the XRD patterns when samples were stored for a couple of
23
24 months, thus suggesting a long term stability in ambient conditions (SI, Figure- S2).



54 **Figure 1.** (a) XRD patterns of Cs₂SnCl₆ and Gd:Cs₂SnCl₆ at different molar doping percentages. (b) Crystal structure
55 of Cs₂SnCl₆ and Gd:Cs₂SnCl₆. Rietveld refinement for (c) Cs₂SnCl₆ and (d) 3 % Gd: Cs₂SnCl₆. (e) Expanded view of
56 the XRD peak corresponding to (220) crystal plane of Cs₂SnCl₆ and Gd:Cs₂SnCl₆. Cs₂SnCl₆, 1% Gd:Cs₂SnCl₆, 2%
57 Gd:Cs₂SnCl₆ and 3% Gd:Cs₂SnCl₆ represent pristine and molar percentages of Gd-doping during the synthesis,
58 respectively. Rietveld refinement plots for 1 % and 2% Gd:Cs₂SnCl₆ are given in supporting information (Figure S1).
59
60
61
62
63
64
65

The UV-vis absorption and PL spectra were recorded to shed light on the effect of doping on the photo-physical properties. Figure 2a & b shows the UV-vis absorption spectra and corresponding Tauc plots for pristine and Gd doped Cs_2SnCl_6 , respectively. The changes in the absorption band edge for doped samples is evident from the UV-visible spectra which extends beyond 320 nm recorded for pristine sample. As the doping percentage increases, the optical band gap extracted from Figure 2b decreases from 3.8 eV (Cs_2SnCl_6) to 3.6 eV (1 % Gd: Cs_2SnCl_6), 3.4 eV (2 % Gd: Cs_2SnCl_6), and 2.8 eV (3 % Gd: Cs_2SnCl_6). Thus, the Gd-doping has a significant effect on the electronic band structure. The DFT calculations using mBJ+ SOC approximations within Wien2K code for the electronic structure of Cs_2SnCl_6 also show a direct band gap of 3.88 eV at Γ (Gamma) point of the Brillouin zone.³⁰

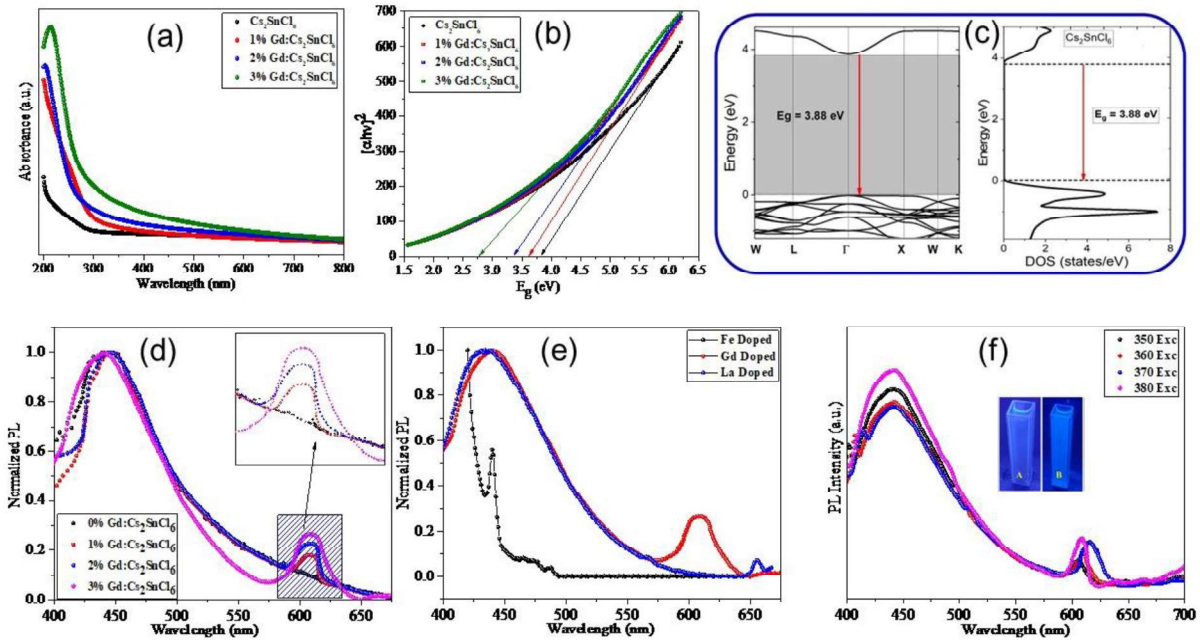


Figure 2. (a) UV-vis spectra of Cs_2SnCl_6 and Gd: Cs_2SnCl_6 at different doping percentages and (b) the corresponding Tauc plots for band gap estimation. (c) Electronic structure and band gap estimated using DFT calculation for Cs_2SnCl_6 . (d) PL spectra of pristine and Gd doped Cs_2SnCl_6 . (e) PL spectra of La, Gd, and Fe doped Cs_2SnCl_6 . (f) PL spectra of 3 % Gd: Cs_2SnCl_6 at various excitation wavelengths. Inset: Photograph of samples under UV-illumination of Cs_2SnCl_6 (left) and 3% Gd: Cs_2SnCl_6 (right). Cs_2SnCl_6 , 1% Gd: Cs_2SnCl_6 , 2% Gd: Cs_2SnCl_6 and 3% Gd: Cs_2SnCl_6 represent pristine and Gd-doped Cs_2SnCl_6 at different molar doping percentages, respectively.

1
2
3
4 Figure 2c shows that the conduction band minimum (mostly populated by Sn-S and Cl- P_z states)
5
6 and valence band maximum (entirely populated by Cl- P_{x-y} states) is located at the same symmetry
7
8 point. Figure 2d shows the PL spectra of pristine and Gd:Cs₂SnCl₆. Cs₂SnCl₆ shows a
9
10 characteristics single emission peak at 440 nm, with a negligible shift towards low energy (from
11
12 438 to 440 nm) when excited at 365 nm.²⁶ The emission centered at 440 nm is asymmetric and has
13
14 an extended tail in the long wavelength region indicating that it originates from the defect states
15
16 rather than from the free excitons of Cs₂SnCl₆. The origin of the 438 nm emission reported earlier
17
18 for Cs₂SnCl₆ is due to the defect states in nanocrystals,²⁶ while the present emission is from the
19
20 bulk microcrystals (> 20 μm, from SEM studies discussed later). As evidenced from the
21
22 crystallographic results, Gd³⁺ is substituted for Sn⁴⁺ site that leads to vacancy states, while charge
23
24 balance is maintained through nonstoichiometric compositions. Further, the elemental analysis and
25
26 XPS studies confirm the successful doping by Gd³⁺ ions (discussed in succeeding sections). Unlike
27
28 the Sb³⁺ doped Cs₂SnCl₆, 3% Gd:Cs₂SnCl₆ does not induce noticeable color change under UV
29
30 illumination. However, Figure 2d clearly shows the emergence of an additional PL emission peak
31
32 which is centered at *ca.* 610 nm. The intensity of the 2nd emission peak increases with the increase
33
34 of the doping percentage (inset of Figure 2d). To clarify the emergence of the 2nd emission, we
35
36 prepared La and Fe- doped DHPs. Interestingly, 5% La:Cs₂SnCl₆ also exhibits a low intensity
37
38 second emission peak at *ca.* 650 nm which is weaker than the emission peak of Gd³⁺- doped DHP,
39
40 while 3% Fe:Cs₂SnCl₆ does not show any second emission peak though showing a distinctly
41
42 different PL emission spectrum (Figure 2e). The low intensity emission from La-doped DHP
43
44 indicates that excitation from the 4f⁰ electron is weak (in the absence of rarely populated 4f
45
46 orbitals) in comparison to the half field 4f⁷-electrons of Gd³⁺- doped DHP. This dual emission
47
48 becomes intense when excited at 380 nm (Figure 2f) which is different from the earlier reports on
49
50
51
52
53
54
55
56
57
58
59
60
61
62
63
64
65

1
2
3
4 doped DHPs where 2nd emission is associated with a change in color, while Gd³⁺- doped DHP
5
6 remains blue under UV-illumination at 365 nm. The photographs of the samples under UV-
7
8 illumination are given as inset in Figure 2f.
9

10
11 The persistence of the 2nd emission peak at 610 nm when varying of the excitation wavelength
12
13 from 350 -380 nm (Figure 2f), indicates that this 2nd emission originates from the Gd³⁺ doping
14
15 rather than overtones of the excitation. It is evident that Gd³⁺- doped DHP exhibits photo-physical
16
17 characteristics different than the emission reported earlier for Sb³⁺, Bi³⁺, or other transition metals
18
19 doping where p orbitals contribute towards the electronic transitions corresponding to singlet
20
21 (¹T_{1u}* → ¹A_{1g}) and triplet (³T_{1u}* → ¹A_{1g}) emissions (such as Bi³⁺ doping) due to a stronger spin
22
23 orbit coupling^{27,29,31} promoted by triplet self-trapped excitations.²⁶ A recent study showed that a
24
25 combination of John-Teller distortion and spin-orbit coupling is responsible for the dual peak at
26
27 cryogenic temperature, while spin-orbit coupling dominates over John-Teller distortion, resulting
28
29 in a single peak in Bi³⁺ doped Cs₂SnCl₆.²⁷ Similarly, the vibrational progression in emission
30
31 spectra at low temperature due to the John-Teller distortion was reported back in 1988 for Cs₂MCl₆
32
33 (M= Zr, Sn).³² Despite the clear understanding of the involvement of p orbitals contributing
34
35 significantly in the origin of band gap and emission process,^{20,31,33} electronic transitions in
36
37 lanthanide doped DHPs involve the 4f-orbitals³⁴ of the dopant, resulting in more complex
38
39 excitation pathways with 4f → 4f transitions, as modeled by the Judd-Ofelt theory, which was later
40
41 extended to 4f → 5d transitions.^{35,36} In general, this type of doping presents broad emission from
42
43 the parity-allowed transition 4f⁶5d¹ → 4f⁷, which presents wide-emission range in the blue-green-
44
45 yellow or red band reported for simple lanthanide ions.^{37,38} The replacement of Sn⁴⁺ with Gd³⁺ in
46
47 the crystal lattice forms molecular orbitals involving Gd, Sn, and Cl that complicates the estimation
48
49 of the electronic band structure responsible for the emission sans a corroboration by theoretical
50
51
52
53
54
55
56
57
58
59
60
61
62
63
64
65

investigation. However, further insights are obtained from the confocal PL imaging of isolated individual emitters and their spectroscopic studies as discussed in the following section.

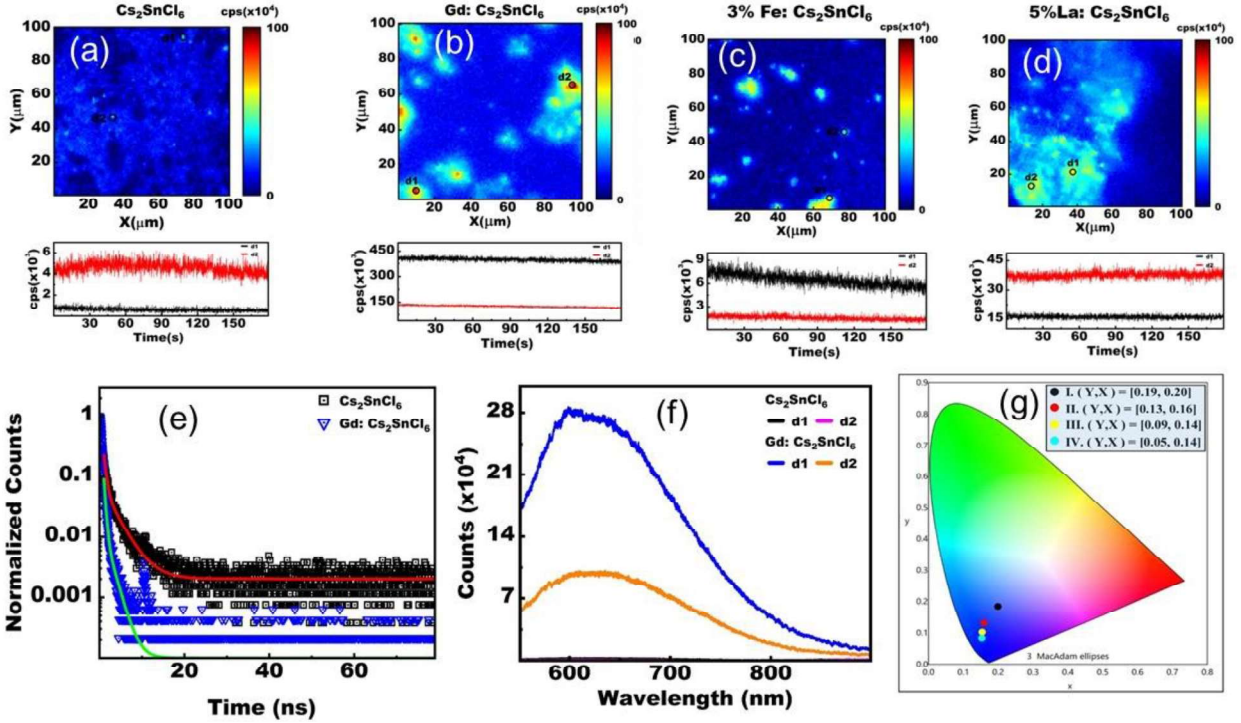


Figure 3. The confocal map (above) and time trace of photons (below) for (a) Cs_2SnCl_6 , (b) 3 % $\text{Gd}:\text{Cs}_2\text{SnCl}_6$, (c) 3 % $\text{Fe}:\text{Cs}_2\text{SnCl}_6$ and (d) 5 % $\text{La}:\text{Cs}_2\text{SnCl}_6$. (e) The PL decay curve of pristine and doped DHPs. (f) PL spectra of Cs_2SnCl_6 and 3 % $\text{Gd}:\text{Cs}_2\text{SnCl}_6$ recorded at selective points of d1 & d2 on the confocal images of the respective DHPs. (g) CIE diagram for pristine and doped DHPs. Coordinates for points I, II, III, and IV represent Cs_2SnCl_6 , 1% $\text{Gd}:\text{Cs}_2\text{SnCl}_6$, 2% $\text{Gd}:\text{Cs}_2\text{SnCl}_6$, and 3% $\text{Gd}:\text{Cs}_2\text{SnCl}_6$, respectively.

In order to carry out confocal imaging studies, the pristine and Gd^{3+} -doped Cs_2SnCl_6 were spread on glass coverslips by drop casting method. All the data presented henceforth are for Cs_2SnCl_6 and 3 % $\text{Gd}:\text{Cs}_2\text{SnCl}_6$, unless mentioned otherwise. Figure 3a and b shows the confocal image of pristine and $\text{Gd}:\text{Cs}_2\text{SnCl}_6$ with a time trace of the photon count intensity (below the confocal map), respectively. The confocal image in Figure 3b shows emission hotspots for $\text{Gd}:\text{Cs}_2\text{SnCl}_6$ from where the photon counts is large, which is absent for the pristine sample (Figure 3a). The data are collected from the emitters located at points d1 and d2 on the confocal image. The time trace shows

1
2
3
4 that the emission is stable at room temperature and does not get photo-bleached which is a good
5
6 signature of emitters useful for quantum photonic and lasing applications.^{39,40}
7
8

9 To verify the emission process, confocal emission images were also recorded for 3% Fe:Cs₂SnCl₆
10 and 5% La:Cs₂SnCl₆. Confocal maps of emitters clearly demonstrate that there was no significant
11 emission from Fe:Cs₂SnCl₆ (Figure 3c), while La:Cs₂SnCl₆ shows emission with lesser photon
12 counts (Figure 3d). The corresponding decay life time and PL spectra are given as supporting
13 information (Figure-S3). It is important to note that minor photon counts (< 9000) recorded for
14 Cs₂SnCl₆ and Fe:Cs₂SnCl₆ may arise due to scattering. Figure 3e and f shows the PL decay and
15 intensity curves for pristine and Gd:Cs₂SnCl₆ originating from isolated individual crystallites. To
16 estimate the PL decay dynamics, experimental data are fitted with a second exponential decay
17 function corresponding to radiative and non-radiative decay process given as:
18
19
20
21
22
23
24
25
26
27
28
29
30

$$31 \quad y = A_1 e^{-x/t_1} + A_2 e^{-x/t_2} \quad \dots (1)$$

32
33
34
35 where t₁ is the lifetime corresponding to the fast-decaying component with A₁ amplitude and t₂
36 corresponds to the slow-decaying component and is related to the tail of the curve with A₂
37 amplitude (y corresponds to entity on y axis i.e. counts and x corresponds to entity on x axis i.e.
38 delay time). The average lifetime is given by the formula:
39
40
41
42
43
44

$$45 \quad \tau_{avg} = \frac{A_1 t_1}{A_1 t_1 + A_2 t_2} t_1 + \frac{A_2 t_2}{A_1 t_1 + A_2 t_2} t_2 \quad \dots (2)$$

46
47
48
49 The doped samples show lower lifetime measured for the 2nd emission (excitation at 532 nm by
50 pulsed diode laser) than the pristine sample (Figure 3e). It indicates that the population of the
51 excited states decreases rapidly (< 1 ns) through a faster radiative decay process for doped
52 Cs₂SnCl₆, while longer decay time recorded for the pristine sample is mostly from the scattering
53 process. The existence of two different decay lifetimes (other one monitored at 440 nm when
54
55
56
57
58
59
60
61
62
63
64
65

excited at 365 nm, Figure-S4, SI) clearly indicates the presence of two or more electronic excitation states of Gd:Cs₂SnCl₆. Figure 3f shows the PL spectra recorded for isolated crystallites of Gd:Cs₂SnCl₆ located at points d1 and d2 on the corresponding confocal PL map while no significant emission is recorded for the pristine sample. The intense PL emission peak is centered around 610 nm, while the PL emission photon counts for the pristine sample are negligible (< 1000, mainly from scattering). Thus, confocal mapping from the individual emitters conclusively confirm the 2nd PL emission centered at *ca.* 610 nm from Gd:Cs₂SnCl₆.

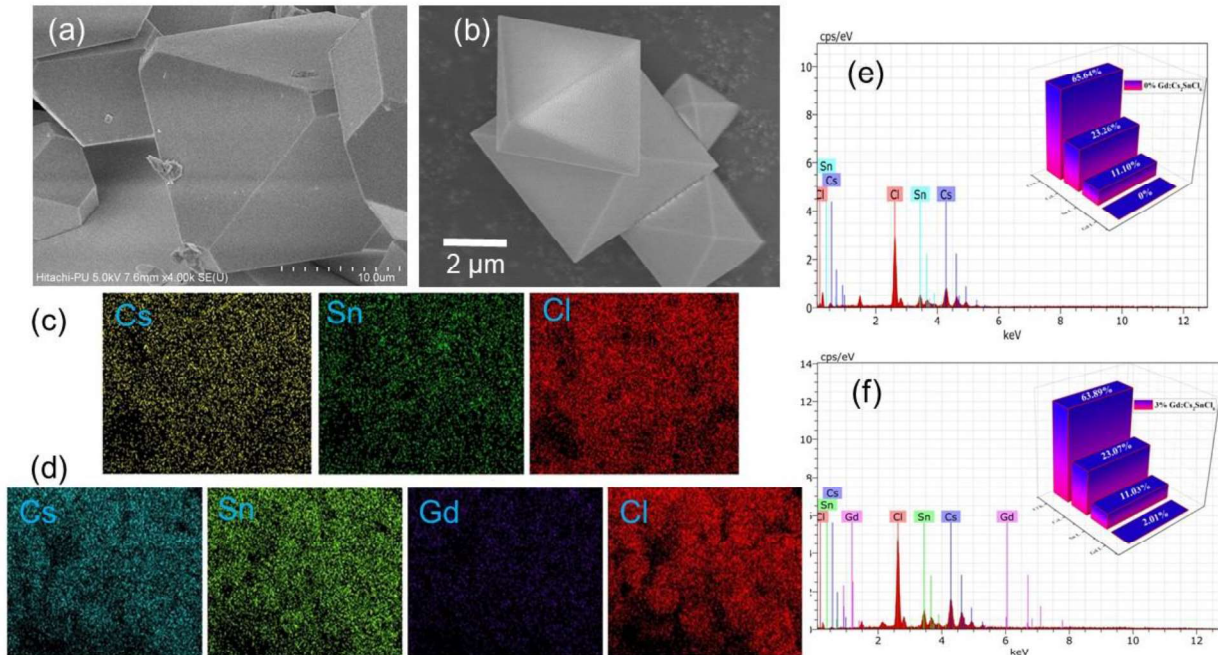


Figure 4. SEM micrographs of (a) Cs₂SnCl₆ and (b) 3 % Gd:Cs₂SnCl₆ DHPs. (c) Elemental mapping for (c) Cs₂SnCl₆ and (d) 3% Gd:Cs₂SnCl₆. EDS of (e) Cs₂SnCl₆ and (f) 3% Gd:Cs₂SnCl₆. Inset: bar diagrams of atomic percentages.

The Commission Internationale de l'Éclairage (CIE) co-ordinates were determined to plot the CIE diagram using Osram software. Figure 3g shows the CIE diagram for pristine and doped Cs₂SnCl₆, while their coordinates are mentioned in the white zone of the figure. As the Gd-content increases, the coordinates marginally shift towards the blue region. Although we have a clear understanding

1
2
3
4 on crystal structure and the PL emission, the morphology and elemental composition of the
5
6
7 crystallites are yet to be studied.

8
9
10 Accordingly, SEM micrographs of pristine and Gd-doped Cs_2SnCl_6 are shown in **Figure 4** along
11
12 with their elemental mapping and EDS profiles. It is evident from the SEM images that pristine
13
14 (Figure 4a) and Gd: Cs_2SnCl_6 (Figure 4b) show large micron sized crystals with truncated
15
16 octahedral shapes. The crystallite size ($< 5 \mu\text{m}$) of Gd: Cs_2SnCl_6 is one fourth of the size to that of
17
18 the pristine DHPs ($> 20 \mu\text{m}$). Similar large bulk crystals have been reported for multi-doped
19
20 Cs_2SnCl_6 synthesized by modified solution growth method.^{26,41} Figure 4c and d shows the
21
22 elemental mappings for pristine and 3% Gd: Cs_2SnCl_6 DHPs, respectively. The elemental mapping
23
24 was carried out for isolated individual crystallites as well. All the elements are uniformly
25
26 distributed throughout the crystal structures. The distribution of elements depends on homogenous
27
28 nucleation of the crystal and effectiveness of the doping. The stoichiometry of the elemental
29
30 composition can be determined by the EDS technique. Figure 4e and f shows the EDS of pristine
31
32 and Gd: Cs_2SnCl_6 , respectively. The presence of Gd^{3+} is confirmed from both elemental mapping
33
34 and EDS of Gd: Cs_2SnCl_6 . The respective elemental compositions are given as inset in the form of
35
36 bar-diagrams. It is clear that no additional elements from the precursor impurity are present. The
37
38 elemental composition analysis is in agreement with the composition analysis from the empirical
39
40 formula of the pristine and Gd: Cs_2SnCl_6 . Similar results are obtained for 1% Gd: Cs_2SnCl_6 and 2%
41
42 Gd: Cs_2SnCl_6 (SI, Figure S5).

43
44
45 In addition, the confirmatory composition analysis was carried by XPS. Figure 5 shows the XPS
46
47 spectra of (a) Sn 3d, (b) Cl 2p, (c) Cs 3d, and (e) Gd 4d electrons for Gd: Cs_2SnCl_6 . XPS spectra
48
49 confirm the presence of Cs ($3d_{5/2}$ 724.1 and $3d_{3/2}$ 738.1 eV), Sn ($3d_{5/2}$ 487.4 and $3d_{3/2}$ 495.9 eV)
50
51 and Cl ($2p_{3/2}$ 198.6 and $2p_{1/2}$ 200.3 eV) in both pristine (Figure S6, SI) and Gd doped DHPs, while
52
53
54
55
56
57
58
59
60
61

the detection of 4d electrons ($4d_{5/2}$ 141.3 and $4d_{3/2}$ 150.6 eV) of Gd^{3+} confirms effective doping in Cs_2SnCl_6 . The results are in agreement with the previous XPS studies on Cs_2SnCl_6 .⁴¹

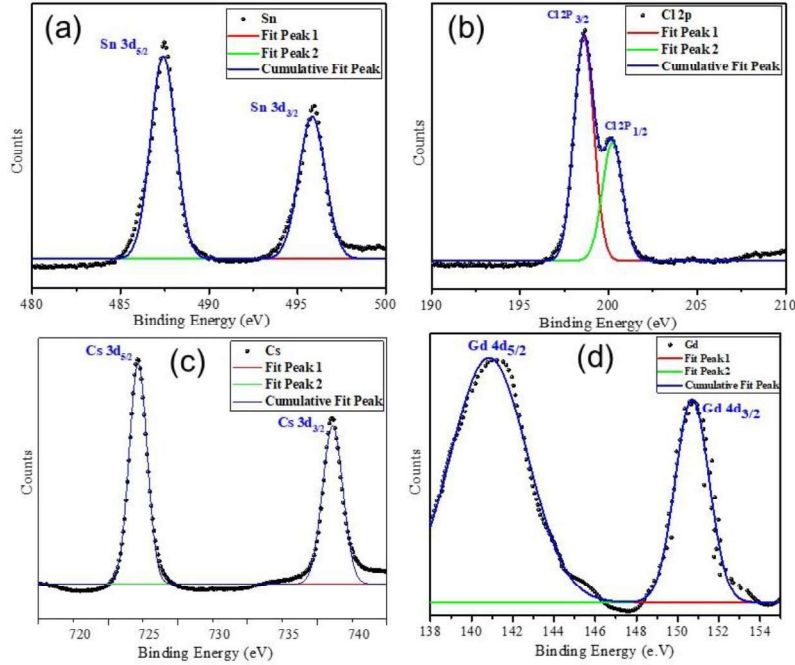


Figure 5. Deconvoluted XPS spectra of (a) Sn 3d, (b) Cl 2p, (c) Cs 3d, and (e) Gd 4d electrons for Gd: Cs_2SnCl_6 DHP. XPS profiles of Sn 3d, Cl 2p, and Cs 3d electrons for the pristine (Cs_2SnCl_6) sample are given as supporting information (Figure-S6).

The experimental evidences presented above confirm the successful synthesis of micron sized crystallites of Cs_2SnCl_6 and Gd doped Cs_2SnCl_6 . Cs_2SnCl_6 shows a single PL emission peak at 440 nm while Gd doping leads to dual emission indicating its application in blue emitting diode.

3. Conclusion

In summary, we have successfully demonstrated the incorporation Gd^{3+} ions in the lead-free double halide perovskite via a simple solvothermal method. Unlike the electronic band structure of Cs_2SnCl_6 when doped by elements with p and d-electrons, lanthanides present much more complex system to simulate for the energy band structure due to the involvement of electrons in f-orbitals and reports on such studies are rare. Despite the complexities involved, incorporation of

1
2
3
4 the gadolinium ions into the crystal lattice enables us to tune the band gap up to 2.8 eV. PL studies
5
6 confirm stable room temperature dual emission at 440 nm and 610 nm from Gd:Cs₂SnCl₆. The
7
8 macroscopic PL emission is strongly supported by confocal PL emission studies. The confocal PL
9
10 emission from the individual crystallites is stable and does not undergo photo bleaching. This
11
12 study will have a significant ramification in developing materials for quantum photonics. Both the
13
14 pristine (Cs₂SnCl₆) and Gd:Cs₂SnCl₆ DHPs exhibit cubic structure with $Fm\bar{3}m$ space group
15
16 having good shelf-life stability. CIE plot shows that Gd:Cs₂SnCl₆ is a better photonic material
17
18 suitable for blue LEDs than Cs₂SnCl₆. SEM studies show the octahedral geometry that results from
19
20 the anisotropic growth of Gd:Cs₂SnCl₆. In brief, our study enhances the experimental
21
22 understanding of the hitherto unknown stable dual emission properties at room temperature upon
23
24 lanthanide doping, leaving a scope for further experimental and theoretical study on the origin of
25
26 the electronic transitions in complex f-electron systems.
27
28
29
30
31
32

33 **4. Experimental Section**

34 **4.1 Chemicals**

35 Cesium chloride (CsCl, Loba Chemie), Tin chloride dihydrate (SnCl₂.2H₂O, Loba Chemie),
36
37 Hydrochloric acid (HCl, 36-38 %, AR grade Loba Chemie), Gadolinium nitrate hexahydrate
38
39 (Gd(NO₃)₃.6H₂O, Sigma Aldrich), Ethanol (absolute, C₂H₆O, Loba Chemie) and Acetone (Loba
40
41 Chemie) were used as received. Deionized water was used for cleansing glassware prior to acetone
42
43 rinsing and drying.
44
45
46
47
48

49 **4.2 Synthesis of Cs₂SnCl₆ and Gd doped Cs₂SnCl₆ DHP**

50
51 2 mmol of CsCl (336.00 mg) and 1 mmol of SnCl₂.2H₂O (225.63 mg) were completely dissolved
52
53 in 5 mL of HCl (light yellow). After sonication for about 5 min, the reaction mixture turned milky
54
55 white. The mixture was transferred into a Teflon lined stainless steel autoclave (50 mL capacity)
56
57 followed by thermal treatment for about 10 hours at 180 °C. The autoclave was cooled down
58
59
60
61
62
63
64
65

1
2
3
4 naturally to ambient temperature and the precipitate was washed with ethanol and acetone several
5
6 times after removing the supernatant. The samples were then dried in a vacuum oven at 50 °C for
7
8 about 12 hours and stored at room temperature for characterization. Required molar quantities of
9
10 gadolinium nitrate were added during the synthesis of 1, 2, and 3 % Gd-doped Cs₂SnCl₆ while
11
12 maintaining the other reaction conditions identical. Appropriate amounts of samples were
13
14 dispersed in ethanol/methanol before drop casting on substrates and for UV-visible spectroscopic
15
16 studies.
17
18
19
20

21 **4.3 Characterisation**

22
23
24 X-ray diffraction (XRD) studies were performed on a Rigaku Miniflex 600 diffractometer.
25
26 Scanning electron microscopy (SEM, JEOL Japan, Model No. JSM 6100) and energy-dispersive
27
28 spectroscopy (EDS, Ultra plus, Model No. 4322, ZEISS) were performed for morphological and
29
30 compositional analysis. Optical studies were carried out on a UV-visible spectrophotometer
31
32 (JASCO, V-770). For photoluminescence, a Horiba Fluorolog Fluorescence Spectrometer
33
34 (Fluorolog 3TCPS) was employed.
35
36
37
38

39 In order to carry out the confocal microscopy studies, the samples were spread on glass coverslips.
40
41 All the samples were dispersed in methanol and sonicated for 30 minutes before drop casting an
42
43 aliquot of 40 µl each. The confocal images were recorded using a home-built laser scanning
44
45 confocal microscope. The 532 nm pulsed diode laser (LDH-D-FA-530L, Picoquant, Germany)
46
47 was used to excite the sample. The excitation was done using a 60X magnification objective
48
49 (Nikon) with a numerical aperture (NA) of 0.95 to get maximum collection efficiency. The
50
51 coverslip containing the sample was mounted on an x-y-z translational stage controlled by
52
53 actuators (M-230.25; Physik Instruments) that allow the spatial scan of the sample. The whole
54
55 setup was controlled by a custom built LabVIEW software program. The setup worked in
56
57
58
59
60
61
62
63
64
65

1
2
3
4 reflecting geometry thus, the emission was collected by the same objective and was accomplished
5
6 by the excitation pulse. In order to filter out the emission counts from excitation (mostly due to
7
8 scattering), a dichroic filter (DF) was used. The signal was further filtered using a long pass (LP).
9
10 The confocal map was recorded using a 660 ± 10 nm spectral filter and the emission was coupled
11
12 with the multimode fiber. The fiber then brought the light to a highly sensitive single photon
13
14 avalanche photodiode (SPAD, Excelitas technology). The lifetime measurements were carried out
15
16 using a time-correlated single-photon counting unit (Hydraharp 400, PicoQuant).
17
18

19
20 The photoluminescence (PL) spectra were recorded using EMCCD (Newton 970, Oxford
21
22 instruments). A grating with a groove density of 900 lines/mm was used for PL spectra acquisition.
23
24 The signals were acquired in EMCCD mode of the spectrometer for 0.1 sec with 20 accumulations.
25
26 It was observed that all samples got photo bleached for laser power above $200 \mu\text{W}$. Thus, for the
27
28 lifetime and PL measurement, the laser intensity was set below this threshold.
29
30
31

32 33 34 **Supporting Information**

35
36 Additional PL spectra, SEM images, XPS, and XRD data are provided as Supporting Information
37
38 and is available from the Wiley Online Library or from the author.
39
40

41 **Acknowledgements**

42
43
44 This study was funded by CEFIPRA through the grant No. 6108-1. Authors acknowledge SAIF
45
46 Panjab University, Chandigarh; IIT Roorkee, Roorkee (for XRD, SEM, XPS, and EDS
47
48 measurements); SAIF Mahatma Gandhi University, Kottayam and SAIF IIT Bombay, Mumbai for
49
50 photoluminescence measurements. RVN acknowledges the financial support from DST-ICPS
51
52 (DST/ICPS/QuST/Theme-2/2019/General), DST-SERB (SB/SJF/2020-21/05), and Swarnajayanti
53
54 Fellowship (DST/SJF/PSA-01/2019-20). The authors are highly thankful to Dr. Shakeel Ahmad
55
56
57
58
59
60
61
62
63
64
65 Khanday for DFT calculations and helpful discussions.

References

1. Fu, Y. *et al.* Metal halide perovskite nanostructures for optoelectronic applications and the study of physical properties. *Nat. Rev. Mater.* **4**, 169–188 (2019).
2. Snaith, H. J. & Hacke, P. Enabling reliability assessments of pre-commercial perovskite photovoltaics with lessons learned from industrial standards. *Nat. Energy* **3**, 459–465 (2018).
3. Li, Z. *et al.* Scalable fabrication of perovskite solar cells. *Nat. Rev. Mater.* **3**, 18017 (2018).
4. Stranks, S. D. & Snaith, H. J. Metal-halide perovskites for photovoltaic and light-emitting devices. *Nat. Nanotechnol.* **10**, 391–402 (2015).
5. Jena, A. K., Kulkarni, A. & Miyasaka, T. Halide Perovskite Photovoltaics: Background, Status, and Future Prospects. *Chem. Rev.* **119**, 3036–3103 (2019).
6. Saparov, B. & Mitzi, D. B. Organic–Inorganic Perovskites: Structural Versatility for Functional Materials Design. *Chem. Rev.* **116**, 4558–4596 (2016).
7. Yang, T., Li, F. & Zheng, R. Recent Progress on Cesium Lead Halide Perovskites for Photodetection Applications. *ACS Appl. Electron. Mater.* **1**, 1348–1366 (2019).
8. An, Y. *et al.* Structural Stability of Formamidinium- and Cesium-Based Halide Perovskites. *ACS Energy Lett.* **6**, 1942–1969 (2021).
9. Gao, Y., Pan, Y., Zhou, F., Niu, G. & Yan, C. Lead-free halide perovskites: a review of the structure–property relationship and applications in light emitting devices and radiation detectors. *J. Mater. Chem. A* **9**, 11931–11943 (2021).
10. Zhu, T., Yang, Y. & Gong, X. Recent Advancements and Challenges for Low-Toxicity Perovskite Materials. *ACS Appl. Mater. Interfaces* **12**, 26776–26811 (2020).
11. Han, P. & Han, K. Recent Advances in All-Inorganic Lead-Free Three-Dimensional Halide Double Perovskite Nanocrystals. *Energy & Fuels* **35**, 18871–18887 (2021).
12. Luo, J., Hu, M., Niu, G. & Tang, J. Lead-Free Halide Perovskites and Perovskite Variants as Phosphors toward Light-Emitting Applications. *ACS*

- 1
2
3
4
5
6
7
8
9
10
11
12
13
14
15
16
17
18
19
20
21
22
23
24
25
26
27
28
29
30
31
32
33
34
35
36
37
38
39
40
41
42
43
44
45
46
47
48
49
50
51
52
53
54
55
56
57
58
59
60
61
62
63
64
65
- Appl. Mater. Interfaces* **11**, 31575–31584 (2019).
13. Pantaler, M. *et al.* Revealing Weak Dimensional Confinement Effects in Excitonic Silver/Bismuth Double Perovskites. *JACS Au* **2**, 136–149 (2022).
 14. Li, B. *et al.* Tin-Based Defects and Passivation Strategies in Tin-Related Perovskite Solar Cells. *ACS Energy Lett.* **5**, 3752–3772 (2020).
 15. Maughan, A. E., Ganose, A. M., Scanlon, D. O. & Neilson, J. R. Perspectives and Design Principles of Vacancy-Ordered Double Perovskite Halide Semiconductors. *Chem. Mater.* **31**, 1184–1195 (2019).
 16. Maughan, A. E. *et al.* Defect Tolerance to Intolerance in the Vacancy-Ordered Double Perovskite Semiconductors Cs₂SnI₆ and Cs₂TeI₆. *J. Am. Chem. Soc.* **138**, 8453–8464 (2016).
 17. Huang, H.-M., Jiang, Z.-Y. & Luo, S.-J. First-principles investigations on the mechanical, thermal, electronic, and optical properties of the defect perovskites Cs₂SnX₆ (X = Cl, Br, I). *Chinese Phys. B* **26**, 96301 (2017).
 18. Chu, Y., Hu, Y. & Xiao, Z. First-Principles Insights into the Stability Difference between ABX₃ Halide Perovskites and Their A₂BX₆ Variants. *J. Phys. Chem. C* **125**, 9688–9694 (2021).
 19. Scott, S. M. *et al.* The thermal stability and consolidation of perovskite variant Cs₂SnCl₆ using spark plasma sintering. *J. Am. Ceram. Soc.* **101**, 2060–2065 (2018).
 20. Xiao, Z. *et al.* Ligand-Hole in [SnI₆] Unit and Origin of Band Gap in Photovoltaic Perovskite Variant Cs₂SnI₆. *Bull. Chem. Soc. Jpn.* **88**, 1250–1255 (2015).
 21. Ullah, S. *et al.* Lead-Free Cs₂SnI₆ Perovskites for Optoelectronic Applications: Recent Developments and Perspectives. *Sol. RRL* **5**, 2000830 (2021).
 22. Wang, A. *et al.* Controlled Synthesis of Lead-Free and Stable Perovskite Derivative Cs₂SnI₆ Nanocrystals via a Facile Hot-Injection Process. *Chem. Mater.* **28**, 8132–8140 (2016).
 23. Li, M. *et al.* Prospective on the Doping Engineering of Vacancy-Ordered Halide Double Perovskites for Enhanced Optoelectronic Properties. *J. Phys. Chem. C* (2022) doi:10.1021/acs.jpcc.2c04502.
 24. Yao, Y. *et al.* Air stable and highly efficient Bi³⁺-doped Cs₂SnCl₆ for blue light-emitting diodes. *RSC Adv.* **11**, 26415–26420 (2021).

25. Das Adhikari, S. *et al.* White light emission from lead-free mixed-cation doped Cs₂SnCl₆ nanocrystals. *Nanoscale* **14**, 1468–1479 (2022).
26. Jing, Y., Liu, Y., Zhao, J. & Xia, Z. Sb³⁺ Doping-Induced Triplet Self-Trapped Excitons Emission in Lead-Free Cs₂SnCl₆ Nanocrystals. *J. Phys. Chem. Lett.* **10**, 7439–7444 (2019).
27. Arfin, H. & Nag, A. Origin of Luminescence in Sb³⁺- and Bi³⁺-Doped Cs₂SnCl₆ Perovskites: Excited State Relaxation and Spin–Orbit Coupling. *J. Phys. Chem. Lett.* **12**, 10002–10008 (2021).
28. Bounos, G. *et al.* Defect Perovskites under Pressure: Structural Evolution of Cs₂SnX₆ (X = Cl, Br, I). *J. Phys. Chem. C* **122**, 24004–24013 (2018).
29. Jin, M. *et al.* Unraveling the triplet excited-state dynamics of Bi³⁺ in vacancy-ordered double perovskite Cs₂SnCl₆ nanocrystals. *Nano Res.* (2022) doi:10.1007/s12274-022-4277-7.
30. Blaha, P. *et al.* WIEN2k: An APW+lo program for calculating the properties of solids. *J. Chem. Phys.* **152**, 74101 (2020).
31. Zeng, R. *et al.* Boosting triplet self-trapped exciton emission in Te(IV)-doped Cs₂SnCl₆ perovskite variants. *Nano Res.* **14**, 1551–1558 (2021).
32. Drummen, P. J. H., Donker, H., Smit, W. M. A. & Blasse, G. Jahn-Teller distortion in the excited state of tellurium(IV) in Cs₂MCl₆ (M=Zr, Sn). *Chem. Phys. Lett.* **144**, 460–462 (1988).
33. Karim, M. M. S. *et al.* Anion Distribution, Structural Distortion, and Symmetry-Driven Optical Band Gap Bowing in Mixed Halide Cs₂SnX₆ Vacancy Ordered Double Perovskites. *Chem. Mater.* **31**, 9430–9444 (2019).
34. Bala, A. & Kumar, V. Stability of the Eu²⁺ Dopant in CsPbBr₃ Perovskites: A First-Principles Study. *J. Phys. Chem. C* **123**, 6965–6969 (2019).
35. Ofelt, G. S. Intensities of Crystal Spectra of Rare- Earth Ions. *J. Chem. Phys.* **37**, 511–520 (1962).
36. Xia, S. & Duan, C.-K. The simple model and its application to interpretation and assignment of 4f–5d transition spectra of rare-earth ions in solids. *J. Lumin.* **122–123**, 1–4 (2007).
37. Jia, Y., Miglio, A., Poncé, S., Mikami, M. & Gonze, X. First-principles study of the luminescence of $\{\mathrm{Eu}\}^{\{2+\}}$ -doped phosphors. *Phys. Rev. B* **96**, 125132 (2017).

- 1
- 2
- 3
- 4
- 5 38. Baran, A. *et al.* Luminescence properties of different Eu sites in
- 6 LiMgPO₄:Eu²⁺, Eu³⁺. *J. Phys. Condens. Matter* **26**, 385401 (2014).
- 7
- 8 39. The rise of integrated quantum photonics. *Nat. Photonics* **14**, 265 (2020).
- 9
- 10 40. Afify, H. A. *et al.* Highly Stable Lasing from Solution-Epitaxially Grown
- 11 Formamidinium-Lead-Bromide Micro-Resonators. *Adv. Opt. Mater.* **10**,
- 12 2200237 (2022).
- 13
- 14
- 15 41. Zhong, Y. *et al.* Multi-Dopant Engineering in Perovskite Cs₂SnCl₆: White
- 16 Light Emitter and Spatially Luminescent Heterostructure. *Inorg. Chem.* **60**,
- 17 17357–17363 (2021).
- 18
- 19
- 20
- 21
- 22
- 23
- 24
- 25
- 26
- 27
- 28
- 29
- 30
- 31
- 32
- 33
- 34
- 35
- 36
- 37
- 38
- 39
- 40
- 41
- 42
- 43
- 44
- 45
- 46
- 47
- 48
- 49
- 50
- 51
- 52
- 53
- 54
- 55
- 56
- 57
- 58
- 59
- 60
- 61
- 62
- 63
- 64
- 65